Synthesis and Characterization of Polyurethane Urea Based on Fluorine-Containing Bisphenoxydiamine

Xiu-Min Qin,[1] Fang Fang,[1] Xiao-Hui Yang,[1] Xin-Ling Wang,[1] Zhen Zheng[1]

School of Chemistry and Chemical Technology, Shanghai Jiao Tong University, 800 Dongchuan Road, Shanghai 200240, People's Republic of China

Received 28 September 2005; accepted 9 January 2006
DOI 10.1002/app.24138
Published online in Wiley InterScience (www.interscience.wiley.com).

ABSTRACT: A fluorine-containing bisphenoxydiamine, 2,2-bis[4-(4-aminophenoxy)phenyl]hexafluoropropane ($BAPF_6P$), was synthesized and characterized by means of Fourier transform infrared spectrometry (FTIR), NMR, and elemental analysis. The obtained $BAPF_6P$ was used as a chain extender to prepare polyurethane urea (PUU), whose morphology and properties were measured through FTIR, differential scanning calorimetry, thermogravimetric analysis, tensile measurements, and atomic force microscopy. The results show that the PUU elastomers based on $BAPF_6P$ exhibited good mechanical properties and thermal stability.
 J Appl Polym Sci 102: 1863–1869, 2006

Key words: elastomers; fluoropolymers; modification; polyurethanes; thermal properties

INTRODUCTION

Polyurethane urea (PUU) and polyurethane (PU) elastomers are multiblock copolymers consisting of two chemically dissimilar alternating segments. In general, the soft segment is polyether or polyester macroglycol, whereas the hard segment forms through the extension of a diisocyanate with a low-molecular-weight diamine or diol. PUU and PU elastomers typically exhibit a two-phase morphology because of the thermodynamic incompatibility between the soft and hard segments. It is the two-phase microstructure that endows these multiblock copolymers with excellent properties, including high tensile strength, high flexibility, and toughness.[1–5] PUU elastomers have relatively higher cohesive urea linkages in the hard segment, and the degree of microphase separation is better than that of corresponding PU elastomers. Therefore, the thermal and mechanical properties of PUU elastomers are superior to those of the conventional PU elastomers.[6,7]

Polymers obtain some special properties if fluorine atoms are introduced into them due to their special characteristics. Some studies on PUU- and PU-containing fluorine have been reported, most of which were patents. Turri et al.[8,9] prepared waterborne PUUs with perfluoropolyether glycol. Kaku et al.[10] prepared a new fluorinated oxazoline block copolymer. Guo and Hunter[11] synthesized a fluorine-containing diol monomer to prepare PU and polyesters. However, rarely has it been reported that fluorine was introduced into the backbones of PUU and PU through the chain extender.

In this study, a kind of novel bisphenoxydiamine containing fluorine, 2,2-bis[4-(4-aminophenoxy)phenyl]hexafluoropropane ($BAPF_6P$), was synthesized, whose chemical composition and characteristics were determined through Fourier transform infrared spectroscopy (FTIR), NMR, and elemental analysis (EA). PUU was prepared with $BAPF_6P$ as the chain extender and was characterized through FTIR, differential scanning calorimetry (DSC), thermogravimetric analysis (TGA), tensile measurements, and atomic force microscopy (AFM). The synthesis and characterization of $BAPF_6P$ are discussed, as well as the synthesis, morphology, and properties of PUU based on $BAPF_6P$.

EXPERIMENTAL

Materials

2,2-Bis(4-hydroxylphenyl)hexafluoropropane (Shanghai 3F New Materials Co., Ltd., Shanghai, People's Republic of China) and 4-chloralnitrobenzene (Shanghai Chemical Reagent Corp., Shanghai, People's Republic of China) was used as received. Toluene diisocyanate (TDI) was used as received from Mitsui Takeda Chemicals, Inc. (Tokyo, Japan). Poly(tetramethylene glycol) (PTMG; DuPont, Inc., Wilmington, DE) with a molecular weight of 1000 was dried *in vacuo* over 100°C for 2 h to remove trace water. *N,N*-Dimethylformamide (DMF; Shanghai Chemical Reagent Corp., Shanghai, China) was distilled *in vacuo*

Correspondence to: X.-L. Wang (xlwang@sjtu.edu.cn).

after it was stirred in anhydrous magnesium sulfate for 3–4 days. Methylene bisorthochloroaniline (MOCA, Suzhou Xiang Yuan Fine Chemicals Co., Ltd., Suzhou, China) was used as received. Ethylene glycol monomethyl ether, hydrazine monohydrate ($H_2NNH_2 \cdot H_2O$; 85%), 1,4-dioxane, anhydrous potassium carbonate (K_2CO_3), methanol, and ethanol were all used as received from Shanghai Chemical Reagent Corp (Shanghai, China).

Synthesis

Synthesis of $BAPF_6P$

Step 1: synthesis of 2,2-bis[4-(4-nitrophenoxy)phenyl] hexafluoropropane. 2,2-Bis(4-hydroxylphenyl)hexafluoropropane (100 g), 4-chloralnitrobenzene (100 g), K_2CO_3 (89.2 g), and DMF (600 mL) were put in a 1000-mL, round-bottom flask equipped with a mechanical stirrer, thermometer, and condenser. After it was kept at 140–150°C for 10 h, the reaction system was cooled to room temperature and then poured into methanol under stirring. One hour later, the crude product was filtered under reduced pressure, washed several times with distilled water, and put in a vacuum oven at 50°C for at least 24 h to obtain a yellowish powder, 2,2-bis[4-(4-nitrophenoxy)phenyl]hexafluoropropane ($BNPF_6P$). The yield was about 75%.
Step 2: synthesis of $BAPF_6P$. The obtained $BNPF_6P$ (0.2 mol), active carbon (10 g), $FeCl_3 \cdot 6H_2O$ (1 g), and ethylene glycol monomethyl ether (250–300 mL) were put into a three-necked flask with a thermometer, mechanical stirrer, and condenser. The system was stirred at 100°C for 0.5 h, and then, $H_2NNH_2 \cdot H_2O$ (85%, 1 mol) was added dropwise. After the addition was finished, the reaction was maintained at 105°C for another 8 h. To prevent the product from separating out, the mixture was heat filtered and then washed with hot ethylene glycol monomethyl ether. The filtrate was neutralized by hydrochloric acid (20%, 300 mL). When white precipitate emerged, ammonia was added to neutralize the excessive hydrochloric acid to a pH value of 11–12. The precipitate was washed several times, recrystallized from anhydrous ethanol, and then put into a 60°C vacuum oven to constant weight. The final product, $BAPF_6P$, was maple powder.

Synthesis of PUUs

Step 1: synthesis of isocyano-capped PU prepolymer. TDI (0.1 mol) was charged into a 250-mL, four-necked round-bottom flask equipped with a thermometer, mechanical stirrer, dropping funnel, and nitrogen inlet, and then, the predried PTMG (0.05 mol) was dropped with a 50-mL constant-pressure dropping funnel. The reaction was maintained at 70–80°C for 2 h to obtain isocyano (NCO)-capped PU prepolymer.
Step 2: preparation of PUU. The —NCO content of PU prepolymer was determined by dibutylamine titration, according to which the exact amount of $BAPF_6P$ as the chain extender was calculated on the basis of [—NCO]/[—H] = 1.05(mol/mol). $BAPF_6P$ was dissolved in 1,4-dioxane and was poured into PU prepolymer; at the same time, more 1,4-dioxane was added to the mixture to obtain a 30 wt % (solid content) solution. Subsequently, the mixture was intensively stirred for several minutes and was vacuum degassed for 10 min. Afterwards, the degassed product was poured into Teflon molds to produce flexible PUU films under room temperature for 24 h. Finally, the film was held in a 110°C oven for 3 h and put into a 60°C vacuum oven for at least 48 h.

PUU films based on MOCA were prepared with a polymerizing process similar to those derived from $BAPF_6P$.

Measurements

FTIR

The FTIR spectra were recorded on a Paragon 1000 instrument (PerkinElmer Co., Wellesley, MA) over the range 4400–450 cm^{-1}.

NMR

^1H-NMR spectrum of $BAPF_6P$ was recorded on Varian DRX 500 NMR spectrometer (Varian NMR Instruments) with the operating frequency at 400 MHz. The solvent was deuterated dimethyl sulfoxide (DMSO-d_6).

EA

Elements analysis of $BAPF_6P$ was performed on 2400 series II CHNS/O analyzer (PerkinElmer, Wellesley, MA).

AFM

AFM of PUUs was recorded with a tapping mode on Nanoscope IIIa scanning probe microscope (Digital Instruments, Inc.). The scanning range was 500 nm, and the scanning frequency was 2 Hz.

DSC

DSC analysis was carried out on a PYRIS DSC analyzer (PerkinElmer, Wellesley, MA) under a dry nitrogen purge. The PUU samples were first heated from room temperature to 250°C to counteract the thermal history; 3 min later, the temperature was reduced to

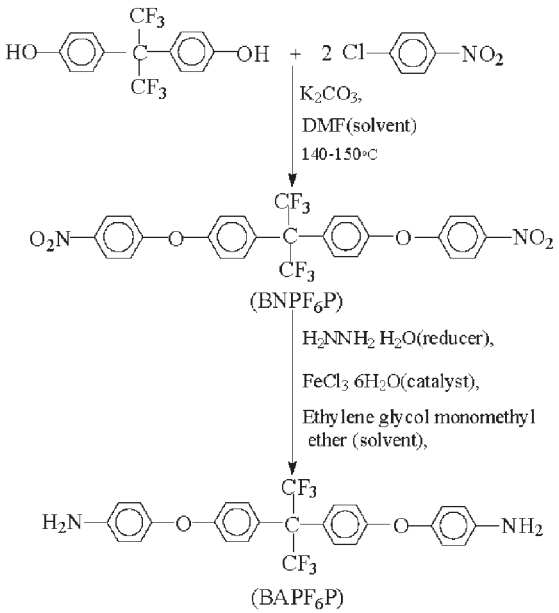

Scheme 1 Synthesis of $BAPF_6P$.

−70°C and then increased to 250°C at a heating rate of 10°C/min. Sample weights were 10–15 mg.

TGA

TGA of the PUU elastomers was performed on a TGA 7 instrument (PerkinElmer, Wellesley, MA) at a heating rate of 20°C/min in a nitrogen atmosphere.

Mechanical properties

The tensile properties of PUU films were investigated with an Instron model 4465 universal testing machine (Instron Corp., Canton, MA). The elongation rate was 500 mm/min with a full load of 10 kg. The specimens were 20 × 4 × 0.5–1 mm. The results reported are the mean values for five replicates. Hardness measurement was carried out with a calibrated Shore A durometer (Shanghai Cary Precision Instrument Co., Ltd., Shanghai, China) at 23°C. All samples were stored in desiccator at room temperature for at least 2 weeks before tensile tests and hardness measurements were performed.

RESULTS AND DISCUSSION

Synthesis, structure, and characteristics of 2,2-bis[4-(4-aminophenoxy)phenyl]hexafluoro-propane

The synthesis of $BAPF_6P$ included two steps (shown in Scheme 1). In the first step, $BNPF_6P$ was prepared, whose synthetic route and chemical structure is also shown in Scheme 1. This step was a nucleophilic substitution reaction. Because of its weak acidity, it was not easy for hydroxybenzene to set free a proton. In this study, K_2CO_3 was applied just to turn hydroxybenzene into a corresponding salt, which could release a proton more easily. In addition, DMF was used as the solvent because solvents with strong polarities can accelerate the separation of a metallic cation from a hydroxybenzene salt. The incorporation of K_2CO_3 and DMF made the nucleophilic substitution easier. In the second step, $BNPF_6P$ was deoxidized to obtain $BAPF_6P$. The input of $H_2NNH_2 \cdot H_2O$ (as the reducing agent) was more than that of $BNPF_6P$ because plenty of nitrogen would put out and take away some $H_2NNH_2 \cdot H_2O$ from the reaction system.

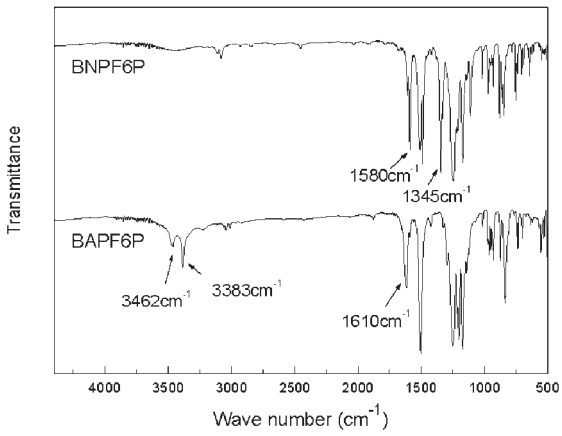

Figure 1 FTIR spectra of 2,2-bis[4-(4-nitrophenoxy)phenyl] hexafluoropropane and $BAPF_6P$.

The structure of the obtained $BAPF_6P$ was identified by FTIR (Fig. 1), NMR (Fig. 2), and EA (Table I).

In Figure 1, the FTIR spectrum of $BNPF_6P$ is also presented, to contrast with $BAPF_6P$. In the spectrum of $BNPF_6P$, there were two strong absorption peaks at about 1580 cm^{-1} (asymmetrical —NO_2 stretch) and 1345 cm^{-1} (symmetrical —NO_2 stretch), which denoted the existence of the —NO_2 function. In the spectrum of $BAPF_6P$, however, the two absorption bands disappeared, and another two sharp strong peaks at

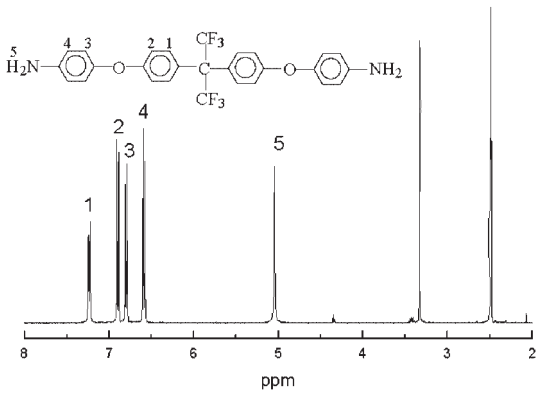

Figure 2 ^1H-NMR spectrum of $BAPF_6P$.

TABLE I
EA Data of $BAPF_6P$

C (%)		H (%)		N (%)		O (%)	
Found	Calcd	Found	Calcd	Found	Calcd	Found	Calcd
62.64	62.55	4.07	3.86	5.30	5.41	6.02	6.18

about 3462 or 3383 cm^{-1} (aromatic N—H stretch) and 1610 cm^{-1} (N—H bend) appeared. This indicated that the —NO_2 in $BNPF_6P$ had been deoxidized to —NH_2.

The ^{1}H-NMR spectrum of $BAPF_6P$ is shown in Figure 2. ^{1}H-NMR spectroscopy showed aromatic protons at δ = 6.571 and 6.593 ppm (d, 4H), 6.783 and 6.805 ppm (d, 4H), 6.885 and 6.907 ppm (d, 4H), and 7.222 and 7.244 ppm (d, 4H), respectively. The peak at 5.041 ppm (s, 4H) was assigned to the protons of —NH_2. The results show that the structure of $BAPF_6P$ agreed with our expectations.

Moreover, EA of $BAPF_6P$ showed good agreement with the theoretical values (Table I), which gave more evidence of its chemical composition.

From the results of FTIR, NMR and EA, we concluded that the chemical structure of the obtained $BAPF_6P$ by this way conformed to our expectations.

The solubility of $BAPF_6P$ is listed in Table II. $BAPF_6P$ was soluble in many polar solvents, including DMF, NMP, and DMSO, although it showed poor solubility in nonpolar solvents. This was easy to understand according to the principle of like dissolves like.

Preparation of PUUs

In this study, PUU was prepared with a two-step method (Scheme 2). At first, the NCO-capped PU prepolymer was synthesized and then chain-extended by $BAPF_6P$ or MOCA. In this study, MOCA was selected as the contrast with $BAPF_6P$ because MOCA is a typical chain extender and is the most used in the preparation of PUU. In the remainder of the article, PUUs based on $BAPF_6P$ and MOCA are designated as FPU and MPU, respectively, unless noted otherwise.

The solidification of FPU films took about 3 h, whereas it took at least 5 h for MPU films to solidify, which showed that the reactivity of $BAPF_6P$ with the PU prepolymer was higher than that of MOCA. This may be attributed to the molecular structure. In MOCA molecules, there are chlorine atoms adjacent to —NH_2 groups. The electrophilic effect and steric hindrance effect of chlorine atoms weakened the reactivity of hydrogen atoms in —NH_2 groups, whereas in $BAPF_6P$, there were no such effects, so the reactivity of MOCA with the NCO-capped PU prepolymer was lower than that of $BAPF_6P$.

In addition, in the preparation of the PUU films, a solvent was added to obtain a polymer solution to cast smooth films because films cast from bulk polymer tend to be rough as a result of the formation of some air bubbles.

The PUU films were held in a 110°C oven for 3 h so that excessive —NCO would react with urethane or urea groups to produce some chemical crosslinked bonds and then produce better mechanical properties.

FTIR analysis of PUUs

The FTIR spectra of the PUUs are displayed in Figure 3. Both of them showed typical absorption bands at 3500–3300 cm^{-1} (N—H stretch), 1800–1600 cm^{-1} (C═O stretch), about 1540 cm^{-1} (C—N stretch and N—H transformation), and 1100 cm^{-1} (C—O stretch). However, there were some little differences between the typical peaks of FPU and MPU. In the spectrum of FPU, the absorption peak of N—H stretch at 3296 cm^{-1} showed that the N—H groups were almost completely hydrogen bonded.[3] In addition, a peak at 1660 cm^{-1}, assigned to hydrogen-bonded urea carbonyl stretch, was found in the spectrum of FPU. In addition, in the spectrum of MPU, a peak at 3350 cm^{-1} appeared due to non-hydrogen-bonded N—H groups. This showed that the hydrogen bonds between the segments of FPU were more than that of MPU.

It is well known that hydrogen bonding can affect the morphology and properties of PUUs.[1,12–15] The differences between the hydrogen bonds distribution of two PUUs reflected the distinction between their morphologies. These differences can be explained ac-

TABLE II
Solubility of $BAPF_6P$

DMF	DMAc	NMP	DMSO	THF	1,4-Dioxane	Acetone	Cyclic hexane	Toluene
○	○	○	○	○	○	□	●	●

○ = soluble; □ = partially soluble; ● = insoluble.

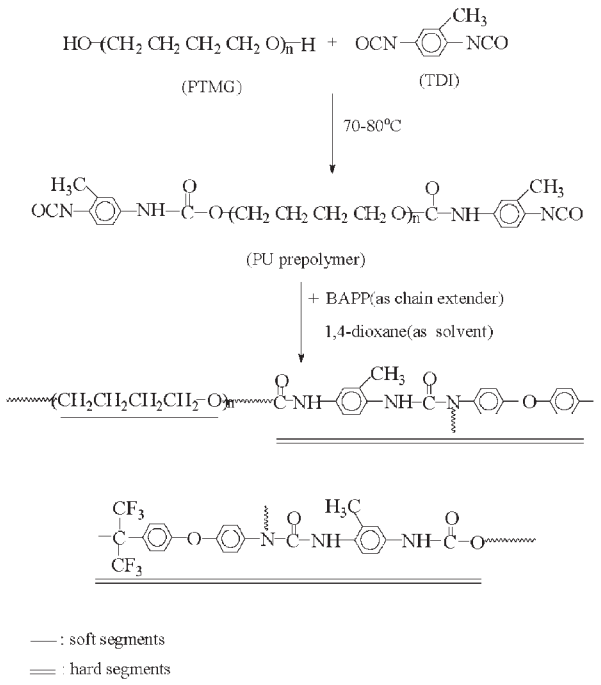

Scheme 2 Preparation of PUU based on 2,2-bis[4-(4-aminophenoxy)phenyl]-hexafluoropropane.

cording to the formation of hydrogen bonding in PUU. N—H groups, as the proton donor, would form hydrogen bonds with not only C—O bond between soft and hard segments but also the urethane and urea C═O between hard segments. In the structure of $BAPF_6P$, there are aromatic C—O bonds and fluorine atoms, which could be the proton acceptors of hydrogen bonds. Then, once $BAPF_6P$ was introduced into the PUU backbones, N—H groups would form hydrogen bonds with these fluorine atoms and C—O bonds and with the C═O bonds between hard segments. Therefore, the introduction of $BAPF_6P$ produced an increase of hydrogen bonds between the hard segments, whereas the hydrogen bond density between

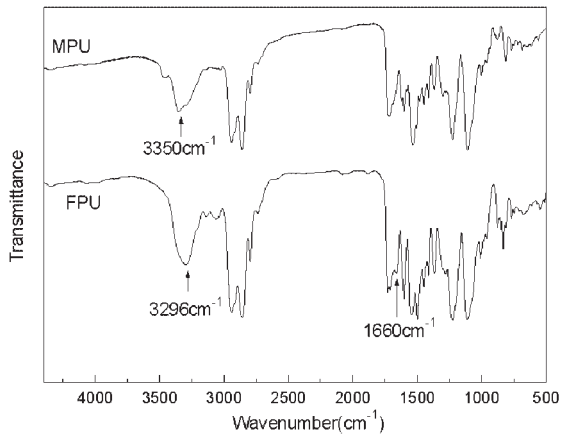

Figure 3 FTIR spectra of the PUUs.

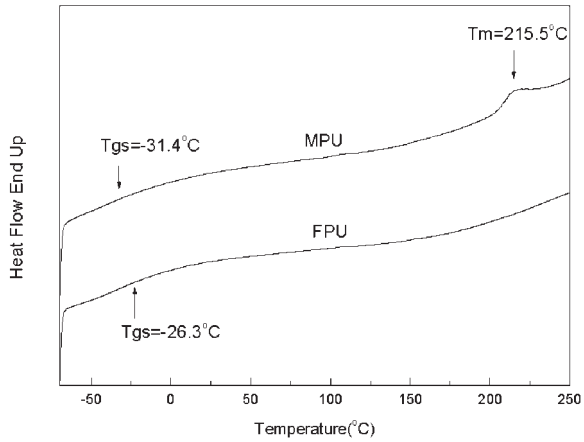

Figure 4 DSC curves of the PUUs (TM: the melting temperature).

the soft and hard segments correspondingly decreased, which usually resulted in an increase in the microphase separation degree.

What is more, the presence of fluorine, which is largely different from the soft segments in solubility parameters, increased phase segregation. Accordingly, we concluded that the incorporation of fluorine caused an improvement in the microphase separation.

DSC analysis of PUUs

The glass-transition temperature of soft segments (T_{gs}) of FPU was a little higher than that of MPU (Fig. 4). This probably resulted from the incorporation of fluorine atoms into the PU backbones. As discussed in the FTIR section, the introduction of fluorine atoms reduced the interaction between the soft and hard segments; in other words, phase separation improved. As a result, the physical crosslinked network, due to the more dispersed hard segment, weakened the flexibility of soft segments, so the T_{gs} was improved.

In addition, as shown in the DSC curve of MPU, a melting peak at 215.5°C appeared, but no such peak was found in the curve of FPU; this showed that there were microcrystallines in MPU, whereas FPU was almost amorphous.

According to previous studies,[16–20] microcrystals can form in PU hard segments on the condition that film is cast from solution. In addition, the crystallinity of PU hard segments is weakened by hydrogen bonding.[15] In this study, it was probably the introduction of fluorine that caused the increase in hydrogen bonding between hard segments, so the crystallinity of FPU was greatly disrupted, which resulted in the amorphism of FPU.

TGA of PUUs

TGA was carried out to provide insight into the thermal stability of PUUs and to measure the decomposi-

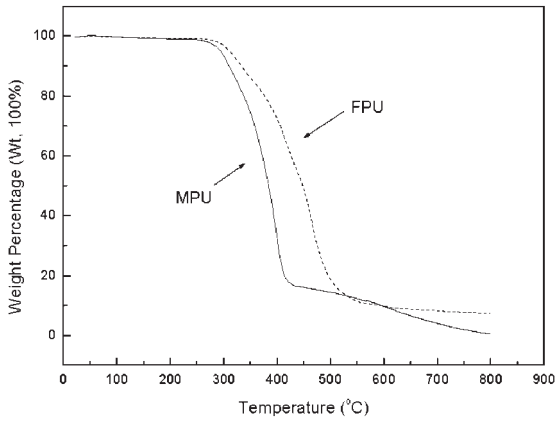

Figure 5 TG plots of the PUUs.

tion temperature. Typical thermogravimetry (TG) and derivative thermogravimetry (DTG) curves of FPU are shown in Figures 5 and 6, respectively. At the same time, the TG and DTG curves of MPU are given as a contrast. Detailed TGA results, including the temperature corresponding to 5% weight loss ($T_{d5\%}$), the temperature corresponding to 50% weight loss ($T_{d50\%}$), and the temperatures of maximum weight loss percentage of each stage (T_{max1}, T_{max2}, and $T_{max1–2}$) are shown in Table III.

According to Table III, the typical temperature values of FPU were higher than those of MPU. Moreover, we concluded from Figure 5 that the thermal degradation rate of FPU was lower than that of MPU, which indicated that the introduction of $BAPF_6P$ into the PU backbone led to a higher thermal stability.

Moreover, the decomposition pattern of FPU was different from that of MPU (Fig. 6). In the DTG curve of MPU, there was just a transitional slope between T_{max1} and T_{max2}, and no $T_{max1–2}$ appeared. It is mainly concluded that the thermal decomposition of PUUs and PUs is initiated from the urethane and urea

TABLE III
TGA Results of the PUUs

Polymer code	$T_{d5\%}$ (°)	$T_{d50\%}$ (°)	T_{max1} (°)	T_{max1-2} (°)	T_{max2} (°)
MPU	295	400	311	—	427
FPU	312	448	332	420	468

groups of hard segments, followed by the degradation of the soft segments, which is a two-stage process.[21–25] According to the DTG curve in Figure 6, however, FPU showed a three-stage degradation pattern, which could probably be explained by its morphology. As discussed previously, the introduction of fluorine caused the hard segments to distribute more evenly into the soft segments, which probably increased the boundary area between the two segments. $T_{max1–2}$ perhaps corresponded to the decomposition of this boundary.

Tensile properties of PUUs

Both FPU and MPU exhibited the tensile properties of typical elastomers (as shown in Fig. 7). As listed in Table IV, the stress at 100% strain, ultimate strength, and break elongation of FPU were higher than that of MPU, whereas the hardness of the former was a little lower.

The properties of PUU imparted by aromatic diamine chain extenders may be explained on the basis of groups present in the diamines. Compared with MOCA, there were fluorine and more rigid benzene rings in the structure of $BAPF_6P$. As discussed previously, the introduction of fluorine and more rigid aromatic rings improved the degree of microphase separation, which would cause hard segments (acting as the physical crosslinks) to distribute more evenly into the soft segments. Consequently, the tensile strength was enhanced.

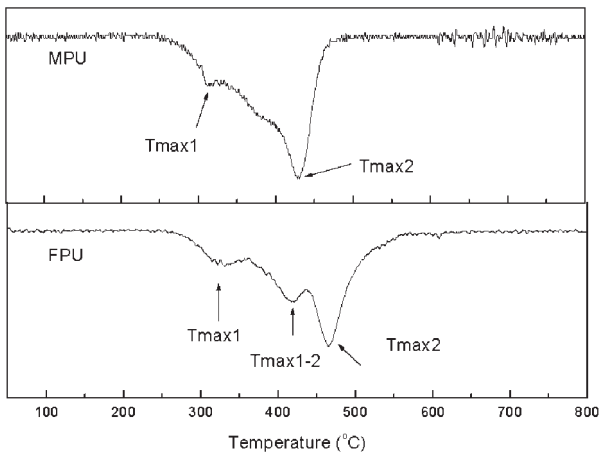

Figure 6 DTG plots of the PUUs.

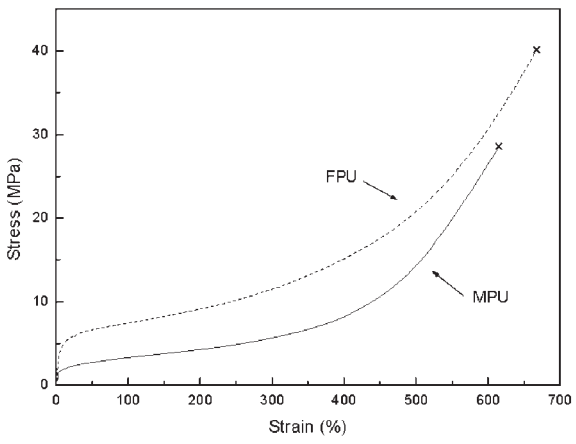

Figure 7 Stress–strain plots of the PUU elastomers.

TABLE IV
Tensile Properties of the PUUs

Polymer	Stress at 100% strain (MPa)	Ultimate strength (MPa)	Break elongation (%)	Hardness (Shore A)
MPU	4.3	30.4	615	76
FPU	7.4	39.5	667	70

AFM of PUs

AFM images of FPU and MPU were shown in Figures 8 and 9, respectively. From Figure 8 and 9, microphase separation could be found in both PUUs, but the hard segment size of FPU was smaller than that of MPU, which caused the hard segments of FPU to distribute more evenly into the soft segments; that is, the area of interface between hard and soft segments became larger. This is just why the T_{gs} of FPU was a little higher than that of MPU, as discussed previously. Furthermore, this sis also the reason that FPU showed better mechanical properties than MPU.

CONCLUSIONS

$BAPF_6P$ was synthesized with a two-step method. The results of FTIR, NMR, DSC, and EA showed that its composition and structure accorded with the expectation.

PUU elastomers were prepared with the obtained $BAPF_6P$ and conventional MOCA as chain-extenders, respectively. The results of FTIR, AFM, and DSC analysis show that the hard microphase of FPU distributed more evenly in the soft microphase than MPU. Compared with MPU, FPU presented a higher thermal stability and mechanical properties, according to the results of DSC, TGA, and stress–strain testing.

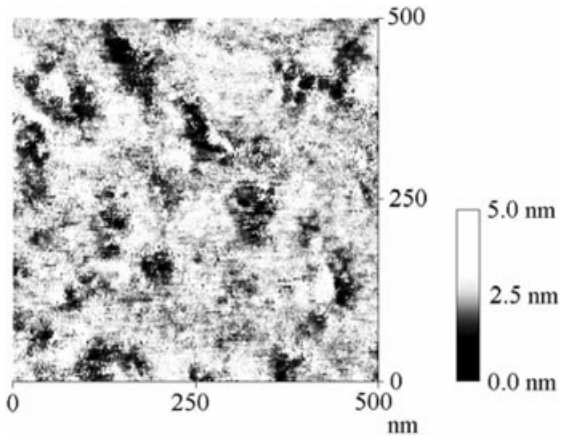

Figure 8 AFM image of FPU.

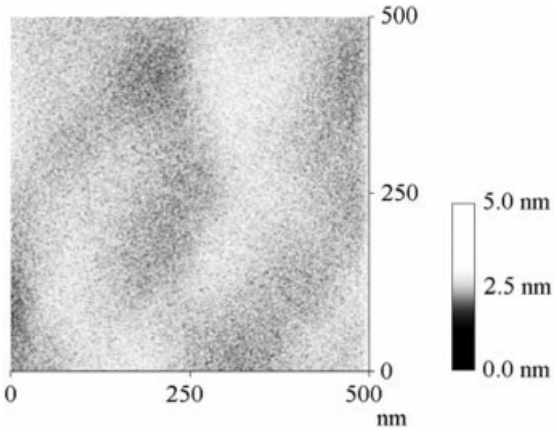

Figure 9 AFM image of MPU.

References

1. Wang, C. B.; Cooper, S. L. Macromolecules 1983, 16, 775.
2. Pomanteer, K. E. Handbook of Elastomers; Bhowmick, A. K.; Stephens, H. L., Eds.; Marcel Dekker: New York, 1998; p 375.
3. Blackwell, J.; Nagarajan, M. R.; Hointnik, T. B. Polymer 1981, 22, 1534.
4. Lai, Y. C.; Quinn, E. T.; Valint, P. L., Jr. J Polym Sci Part A: Polym Chem 1995, 33, 1767.
5. Cheong, I. W.; Kong, H. C.; An, J. H.; Kim, J. H. J Polym Sci Part A: Polym Chem 2004, 42, 4353.
6. Paik Sung, C. S.; Hu, C. B.; Wu, C. S. Macromolecules 1980, 13, 111.
7. Wilkes, G. L.; Abouzahr, S. Macromolecules 1981, 14, 456.
8. Turri, S.; Levi, M.; Trombetta, T. J Appl Polym Sci 2004, 93, 136.
9. Turri, S.; Levi, M.; Trombetta, T. Macromol Symp 2004, 218, 29.
10. Kaku, M.; Grimminger, L. C.; Sogah, D. Y.; Haynie, S. I. J Polym Sci Part A: Polym Chem 1994, 32, 2187.
11. Guo, X. A.; Hunter, A. D. J Polym Sci Part A: Polym Chem 1993, 31, 1431.
12. Koleman, M. M.; Lee, K. H.; Skrovanek, D. J.; Painter, P. C. Macromolecules 1986, 19, 2149.
13. Yamamoto, T.; Shibayama, M.; Nomura, S. Polym J 1989, 21, 895.
14. Hartmann, B.; Duffy, J. V.; Lee, G. F.; Balizer, E. J Appl Polym Sci 1988, 35, 1829.
15. Xiu, Y. Y.; Zhang, Z. P.; Wang, D. N.; Ying, S. K.; Li, J. K. Polymer 1992, 33, 1335.
16. Herrell, L. L., Jr. Macromolecules 1969, 2, 607.
17. Samuels, S. L.; Wilkes, G. L. J Polym Sci Part Polym Lett Ed 1971, 9, 761.
18. Wilkes, G. L.; Samuels, S. L.; Crystal, R. J Macromol Sci Phys 1974, 10, 203.
19. Kimura, I.; Ishihara, H.; Yoshihara, N.; Nomura, S.; Ranai, H. Macromolecules 1974, 7, 355.
20. Briefer, R. M.; Thomas, E. L. J Macromol Sci Phys 1983, 22, 509.
21. Liu, J.; Ma, D. Z. J Appl Polym Sci 2002, 84, 2206.
22. Liu, J.; Ma, D. Z.; Li, Z. Eur Polym J 2002, 38, 661.
23. Lin, M. F.; Shu, Y. C.; Tsen, W. C.; Chuang, F. S. Polym Int 1999, 48, 433.
24. Liu, J.; Ma, D. Z.; Chen, X. M. Acta Polym Sinica 2002, 2, 221.
25. Petrovic, Z. S.; Zavargo, Z.; Flynn, J. H.; MacKnight, W. J. J Appl Polym Sci 1994, 51, 1087.